SYNTHESIS OF CeO$_2$ NANOPARTICLES ON THE MESOPOROUS SILICA SUPPORT *VIA* NANOCASTING

F. VAJA (DUMITRU)[a,b], O. OPREA[a*], D. FICAI[a], A. FICAI[a], C. GURAN[a]
[a]*"Politehnica" University of Bucharest, Faculty of Applied Chemistry and Material Science, Bucharest, Romania*
[b]*Research Institute for Advanced Coatings-ICAA,Bucharest*

In this paper, we describe the synthesis of CeO$_2$ nanoparticles by nanocasting route on the mesoporous silica support. In the first step, mesoporous silica (SBA-15 structure) was prepared using a soft template and in the second step, this material was used for impregnation with CeO$_2$ nanoparticles. The obtained nanocomposites were morphologically and structurally characterized by XRD diffraction, FT-IR, UV-Vis and PL spectra.

1. Introduction

Cerium (Ce) is a member of the lanthanide series and is one of the most abundant of the rare earth elements. In earth's crust it is present at about 66 parts per million as a free metal or oxide form and is more abundant than copper (60 ppm) or tin (2.3 ppm) [1-2]. The two main oxidation states of cerium are cerous-Ce (3$^+$) and ceric-Ce (4$^+$). These oxidation states can auto regenerate, and cerium can switch from one state to other. This is partially due to the similar energy of the 4f and 5d electronic states and low potential energy barrier to electron density distribution between them. Cerium in these oxidation states strongly absorb ultraviolet light. Cerous Ce (3$^+$) absorbance is in the 230–260 nm range and cerium (4$^+$) absorbance is in the 300–400 nm range. *The oxygen storage capacity* (OSC) of ceria, is closely linked to how easily the cerium can change oxidation states [3].

The valence and defect structure of CeO$_2$ is dynamic and may change spontaneously or in response to physical parameters such as temperature, oxygen partial pressure, and doping with other ions [4] as well as an electrical field or surface stresses [5].

CeO$_2$ crystallizes in the fluorite crystal structure with space group *Fm3m* over the temperature range from room temperature to the melting point. The fluorite structure consists of a face-centred cubic (f.c.c.) unit cell of cations with anions occupying the octahedral interstitial sites. In this structure, each cerium cation is coordinated by eight nearest-neighbour oxygen anions, while each oxygen anion is coordinated by four nearest neighbour cerium cations [6]. The colour of CeO$_2$ is pale yellow, probably due to Ce(IV)–O(II) charge transfer. Ceria in the fluorite structure exhibits a few defects depending on partial pressure of oxygen, which is the intrinsic property for its potentials in catalysis, energy conversion and other applications.

Cerium oxide (CeO$_2$) has many applications as a catalysts *e.g.* for the elimination of toxic auto exhaust gases, oxygen sensors, fuel cells, glass-polishing materials, ultraviolet absorbent, etc.

---

*Corresponding author: ovidiu73@yahoo.com

[7,8]. With a decrease in particle size, high densities of interfaces in nanocrystalline solids is obtained.

S.S. Lee *et al.* have recently demonstrated that ceria nanoparticles possess also antioxidant activity at physiological pH values and has potential uses in biomedical applications, such as protection against radiation damage, oxidative stress and inflammation.

The methods used till now to prepare CeO_2 nanoparticles and films include hydrolysis, precipitation, thermal deposition, combustion or flame-synthesis, sol–gel, hydrothermal or solvothermal, sonochemical synthesis, electrochemical synthesis and so on [9,16].

Unfortunately, these techniques are based mainly on high pressure and the sizes of obtained ceria particles are relatively large. Therefore, a simple approach technique for controlled growth of ceria nanostructures is for now essential.

The nanocasting pathway with hard templates opens the door to the design of highly porous solids with multifunctional properties and interesting application perspectives [17]. Nanocasting is a process in which a template with relevant structures on the length scale of nanometers is filled with another material to be cast or a precursor for it, and the initial template is subsequently removed [17]. The group of Ryoo applied the nanocasting method for CeO_2 using uniform mesoporous silica as a hard template for the first time. This method allowed synthesis of highly ordered thermally stable mesoporous CeO_2 with nanocrystalline walls [18]. Recently, Ji *et al.* also prepared ordered mesoporous CeO_2 by nanocasting from cubic *Ia3d* mesoporous MCM-48 silica [19]. The obtained mesoporous CeO_2 has a high density of surface vacancies due to the controlled nanocrystals size.

In this work, we investigate the formation of cerium oxide nanoparticles inside mesoporous silica (SBA-15) matrix.

2. Experimental

2.1 Materials and preparation of nanoparticles

The CeO_2/SBA-15 nanocomposite was prepared by incorporating $Ce(NO_3)_3 \cdot 6H2O$ precursor into the channels of mesoporous silica SBA-15 and subsequent calcination (figure 1). Parent mesoporous silica SBA-15 was synthesized according to the reported process [20].
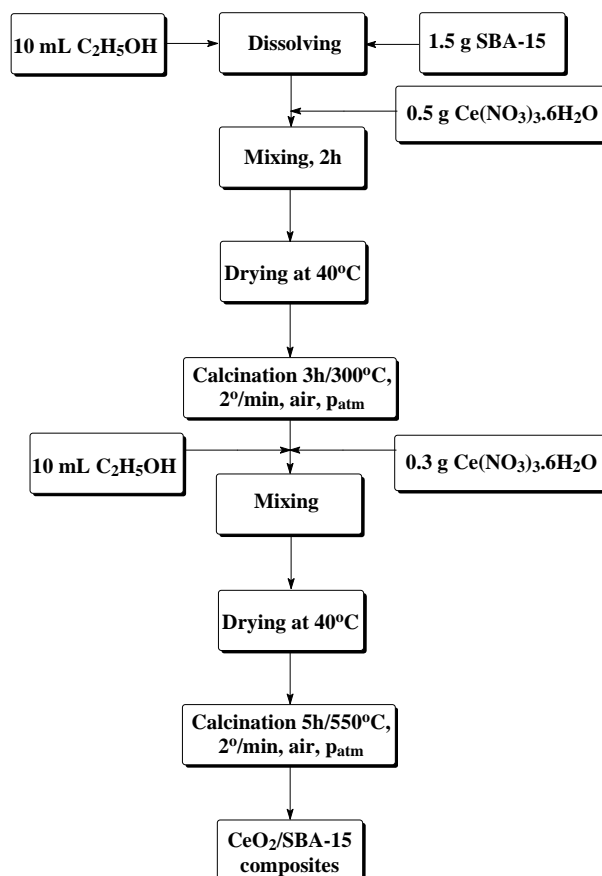
Fig. 1 The procedure of incorporating CeO$_2$ into the channels of SBA-15

In brief, synthetic procedure was carried out as follows: 6g of triblock copolymer Pluronic P123 was mixed with 30 g of hydrochloric acid (HCl) 35 % and 180 mL of deionized water. The mixture was stirred at 35°C until P123 was completely dissolved. A total of 13.5 mL of tetraethyl orthosilicate (TEOS) was added to this solution under vigorous stirring. The final mixture was stirred at 35°C for 24 h, then transferred into an autoclave and kept in the autoclave at 90°C for 24 h under static condition for hydrothermal treatment. Finally, the obtained white precipitates were filtered, washed with water for several times and dried at room temperature. The SBA-15 was obtained by calcining the dried product at 550°C for 4h at a heating rate of 1 C/min in air. In this way, the organic surfactant P123 was removed.

The procedure of incorporating CeO$_2$ into the channels of SBA-15 is according to [21]: 1.5g of mesoporous silica was dissolved in in 10 mL ethanol, then 0.5g Ce(NO$_3$)$_3$·6H2O was added to this solution and stirred for 2 h. The resultant mixture was dried at 40°C and calcined at 300°C for 3h. Next, 10 mL ethanol was added to the dried powder again and stirred, then 0.3g Ce(NO$_3$)$_3$·6H2O was added to the solution. The resultant mixture was dried at 40°C and calcined at 550°C for 5h.

2.2 Characterization techniques

In order to characterize the obtained CeO$_2$/SBA-15 composites a series of analyses were performed: X-ray diffraction, FT-IR , UV-Vis and PL spectrometry.

For *X-ray diffraction* studies was used a Bruker D8 Advance in the 2θ range 10–80°. A scan rate of 1° min^{-1} was employed.

FT-IR spectra were recorded using the KBr pellet technique on a Karl Zeiss Jena UR20 and EQUINOX 55 spectrometer in the 4000–400 cm^{-1} frequency range. A total of 30 scans and a resolution of 1 cm^{-1} were employed in getting the spectra.

Diffuse reflectance spectra measurements were made with a JASCO V560 spectrophotometer with solid sample accessory, in the domain 200-850nm, with a speed of 200 nm·min^{-1}.

Photoluminescence spectra (PL) were measured with a Perkin Elmer P55 spectrometer using a Xe lamp as a UV light source at ambient temperature, in the range 200-800 nm, with all the samples in solid state. The measurements were made with scan speed of 200 nm·min^{-1}, slit of 10 nm, and cut-off filter of 1%. An excitation wavelength of 320 nm was used.

3. Results and discussion

The SBA-15 crystalline phase formation and CeO$_2$/SBA-15 composite were investigated by X-ray diffraction. The XRD pattern for the SBA-15 nanopowder is presented in figure 2, while for CeO$_2$/SBA15 composites the XRD pattern is shown in figure 3.

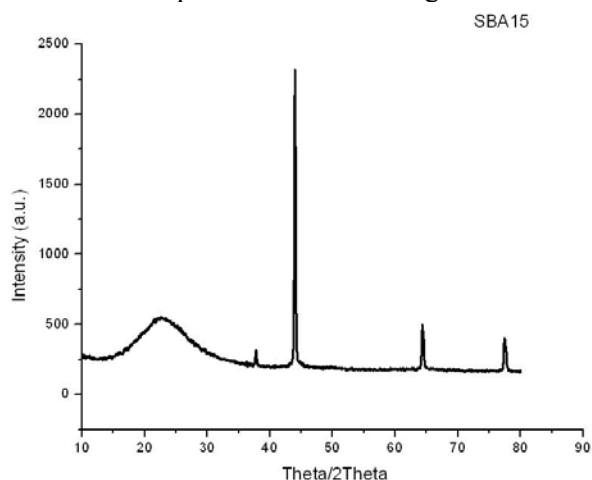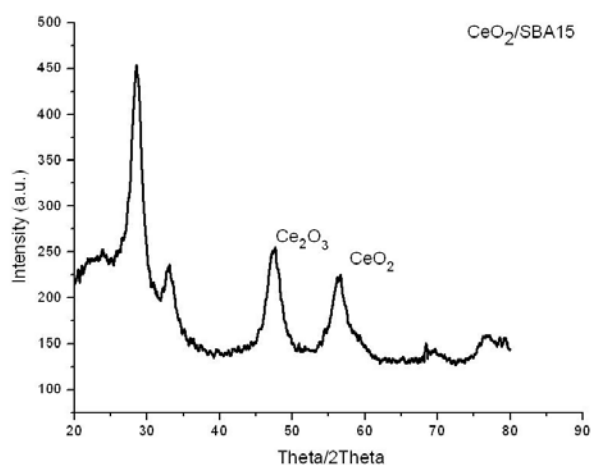*Fig. 2. XRD diffractogram of SBA15*

Fig. 3. XRD diffractogram of CeO$_2$/SBA15 composites

The wide-angle XRD pattern of CeO$_2$/SBA15 prepared by nanocasting method show the peaks at 2θ at 28° (111), 33° (200), 47° (220), 56° (311), 69° (400) and 75° (331) which corresponding to CeO$_2$ and indicates a highly dispersion of the cerium dioxide on the surface of channel wall when introducing cerium species into SBA-15 [22]. The sizes of CeO2 nanoparticles on the mesoporous substrate were calculated using Scherrer's equation:

$$d = \frac{K \times \lambda}{\beta \times \cos\theta}$$

where d is the average grain size, K is set to be 0.89 for normal, λ is the wavelength of X ray(1.54184 Å), β is the half width of the diffraction peak and θ is the Bragg diffraction angle.
From this equation, the calculated crystallite size for the synthesized CeO$_2$ is about 7,2 nm. The intensity of characteristic peaks of SBA15 decreases due to the pore-filling effect of CeO$_2$ particles that reduces the scattering contrast between the pores and the framework of SBA-15 [22].

In order to understand the structural evolution of the nanocasting process FT-IR spectra were recorded for all samples. The FT-IR spectra of pure silica SBA15 and CeO₂/SBA15composites synthesized by nanocasting method are shown in figure 4. The samples presents a characteristic band at ~3400 cm^{-1} that is assigned to the vibration of silanol groups (Si–O–H) situated inside the channels of SBA-15 and surface water molecules [23]. The peak at 1634 cm^{-1} also corresponds to water molecules adsorbed on the nanoparticle's surface.
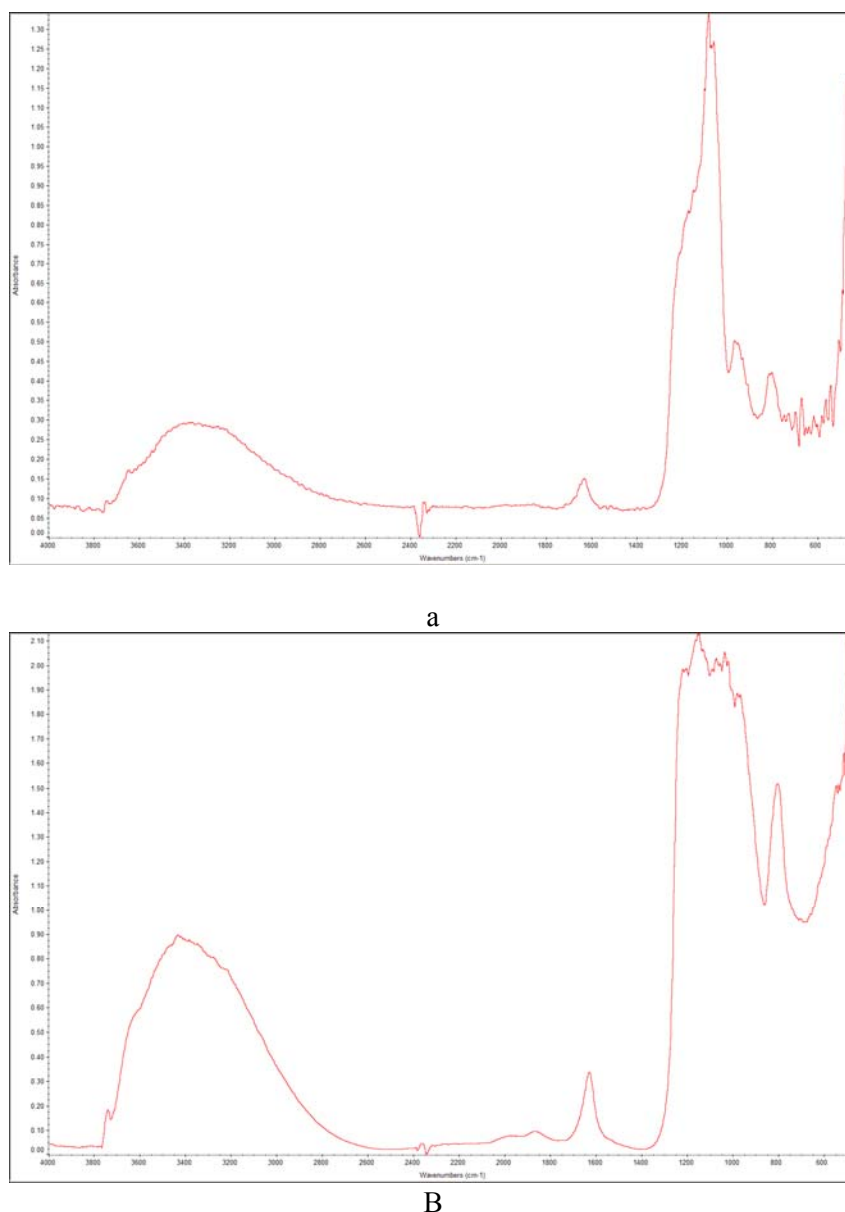

a

B

Fig. 4. FTIR spectrum of a) SBA15 and b) CeO₂/SBA15

The vibration band at ~1090 cm^{-1} is assigned to υ_{as} (Si–O–Si) and its wavenumber decreases with increasing of the cerium content in Ce-SBA15, thus it is observed that the peak at 1090 cm^{-1} in SBA15 shifts to 1087cm^{-1} in Ce/SBA15. The band at ~960 cm^{-1} observed in the pure silica SBA15 sample, can be assigned to the stretching vibrations of Si-O in the Si–O-–R+ groups [23]. With increase of the cerium content in the framework of SBA15, the intensity of peak at 960 cm^{-1} decrease, this implies that Si–O–R or Si–OH groups are changed or consumed and transformed to the Si–O–Ce bonds [23,24].

The UV-vis absorbance of bulk CeO₂ originates from a charge transfer transition from O *2p* to Ce *4f*, and the spectrum (Figure 5) displays two overlapping absorption peaks attributable to

indirect and direct transitions. Usually the absorption edge energy is calculated under the assumption of both a direct and an indirect transition (328 and 258nm) [24,25].
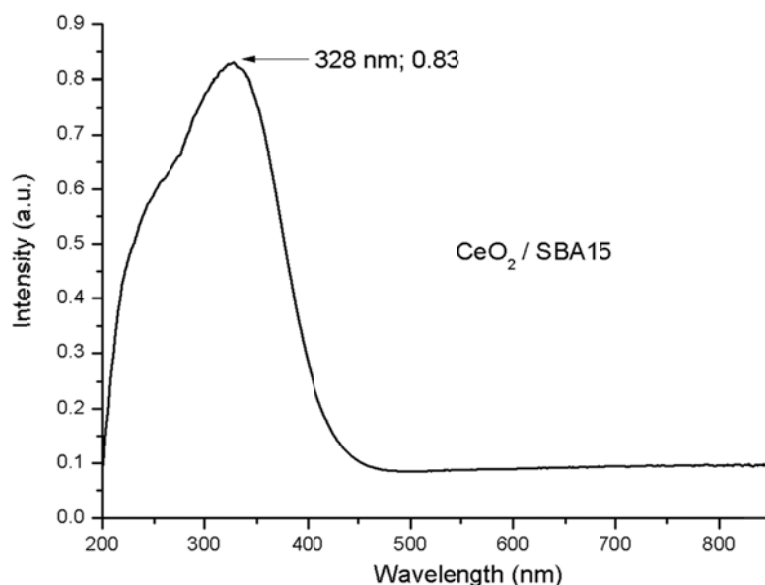

Fig. 5. UV-Vis absorbtion spectra of CeO₂/SBA15 composites

In order to obtain the band-gap energy an intercept with the abscissa from a linear regression of $[(F(R)) \cdot h\upsilon]^{1/n}$ data plotted versus $h\upsilon$, with $n = 1/2$ for a direct transition (figure 6a) and $n = 2$ for indirect transition (figure 6b) was done [25]. The values obtained for $CeO_2/SBA15$ composite are $E_{dir} = 3.317eV$ and $E_{ind} = 2.934eV$. It has been reported that an inverse relationship exists between particle size and absorption edge energy attributable to quantum size effects [26]. It was found that at the outermost nanocrystals surface, Ce^{4+} ions coexist with Ce^{3+} ones when the cluster sizes decrease, the amount of Ce^{3+} increases. At the same time, there is an electrostatic potential effect due to a cerium valence change, which results in the blue shift of the band gap. The bulk CeO_2 has a band gap value of ~3.1eV. As expected for small particles the quantum confinement will increase this value. According to the literature, the band gap energy of ~3.31eV corresponds to a particle size of 7-8 nm, which is in good agreement with the XRD data presented above [26].
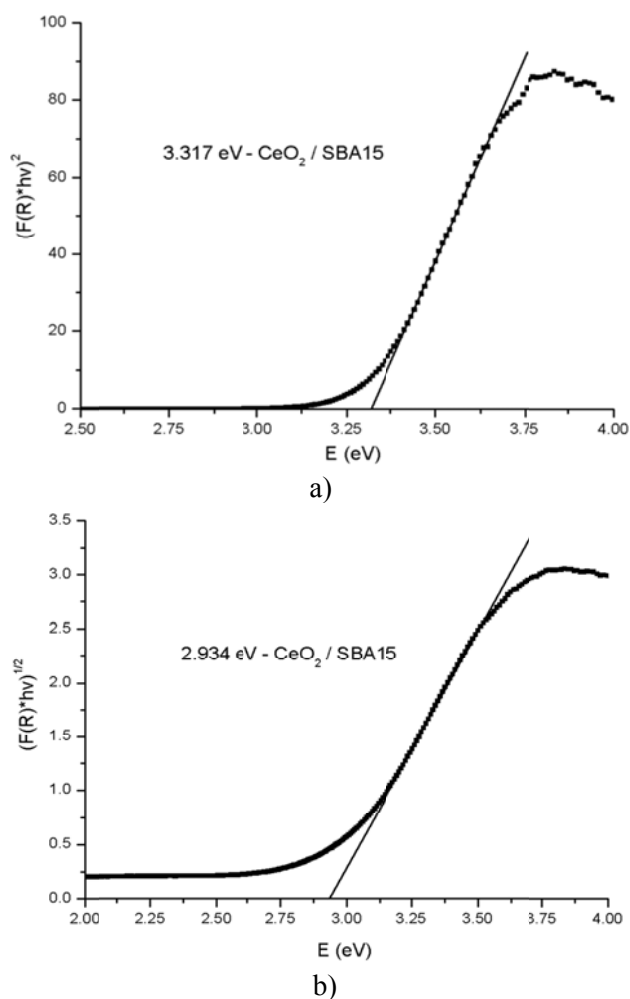
a)

b)

Fig. 6 Determination of the edge energy value (a) direct transition (b) indirect transition
for CeO$_2$/SBA15 composites

The PL spectra of CeO$_2$/SBA15 composite (figure 7) presents a series of emission bands in the domain 375-550nm. The first band, situated in the UV, with maximum at 394nm can be attributed to the excitonic recombination corresponding to the near-band edge emission of CeO$_2$ [26]. The weak green emission band with maximums at 514 and 525 nm may be attributed to the low density of oxygen vacancies during synthesis of CeO$_2$/SBA15 composite [27].
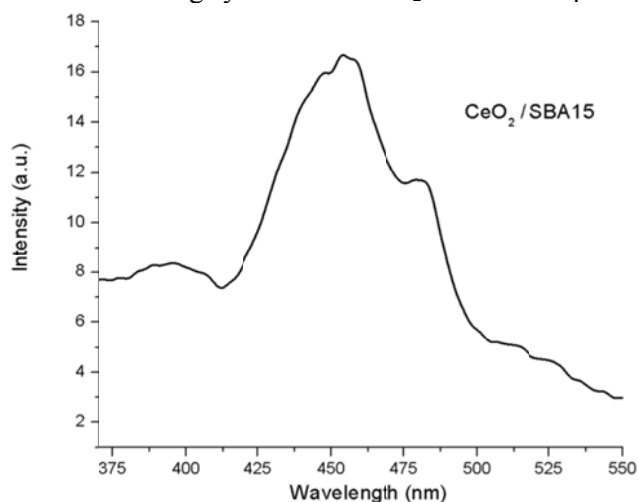

Fig. 7. Photoluminescence spectra of CeO$_2$/SBA15 composites

The emission bands ranging from 400 to 500 nm for CeO_2 sample are attributed to the hopping from different defect levels of the range from Ce 4f to O 2p band [27] and are quite common among other oxides as well [28-32]. The formation of a V_O^{++} luminescent centre by recombination of surface trapped hole with an electron in deep trap (V_O^{+}) gives rise to visible emission when a conduction band electron recombines with the V_O^{++} centre [33]. This explains also the common shape of the emission spectra in 400-500 nm range for the above-mentioned oxides.

4. Conclusion

In this work we have synthetized successfully CeO_2/SBA15 composite by nanocasting method using the ordered mesoporous silica SBA15 as template.

The CeO_2 has been well dispersed in mesoporous silica, the particle size of CeO_2 being smaller than that pore size of the mesoporous silica. The shift of the FT-IR absorption peaks toward the lower wave number is an indication of Ce incorporating into the framework of silica SBA15. The nanocasting strategy can keep the ordered mesostructures of SBA15 whose thermal and hydrothermal stability is higher than another mesoporous templates. As results from our studies, the nanocasting is a method that can be used to prepare nanostructured materials, especially nanomaterials, which are difficult obtained by other synthetic method.

Acknowledgement

References

[1] Z. Y. Hu, S. Haneklaus, G. Sparovek, E. Schnug, Commun. Soil Sci. Plan. **37**, 1381 (2006).
[2] Chunwen Sun, Hong Li and Liquan Chen, Energy Environ. Sci., **5**, 8475 (2012)
[3] J. P. Holgado, R. Alvarez and G. Munuera, Appl. Surf. Sci., **161**, 301 (2000)
[4] G. S. Herman, Surf. Sci. **437**, 207 (1999)
[5] P. Gao, Z. Kang, W. Fu, W. Wang, X. Bai, J. Am. Chem. Soc., **132**, 4197 (2010).
[6] K. Schwarz, Proc. Natl. Acad. Sci. U. S. A., **103**, 3497 (2006).
[7] C. W. Sun, R. Hui, J. Roller, J. Solid State Electrochem., **14**, 1125 (2010).
[8] C. W. Sun, U. Stimming, J. Power Sources, **171**, 247 (2007).
[9] M. Hirano, M. Inagaki, J. Mater. Chem., **10**, 437 (2000).
[10] F. Zhang, Q. Jin, S. W. Chan, J. Appl. Phys., **95**, 4319 (2004).
[11] M. Kamruddin, P. K. Ajikumar, R. Nithya, A. K. Tyagi and B. Raj, Scr. Mater.,
    50, 417 (2004).
[12] R. D. Purohit, B. P. Sharma, K. T. Pillai, A. K. Tyagi, Mater. Res. Bull., **36**, 2711 (2001).
[13] L. Madler, W. J. Stark, S. E. Pratsinis, J. Mater. Res., **17**, 1356 (2002).
[14] C. Laberty-Robert, J. W. Long, E. M. Lucas, K. A. Pettigrew, R. M. Stround, M. S. Doescher
    D. R. Rolison, Chem. Mater., **18**, 50 (2006).
[15] L. Yin, Y. Wang, G. Pang, Y. Koltypin, A. Gedanken, J. Colloid Interface Sci.,
    246, 78 (2002).
[16] Y. Zhou, R. J. Phillips, J. A. Switzer, J. Am.Ceram. Soc., **78**, 981 (1995).
[17] A. H. Lu, F. Schuth, Adv. Mater., **18**, 1793 (2006).
[18] S. C. Laha and R. Ryoo, Chem. Commun., 2003, p. 2138.
[19] P. Ji, J. Zhang, F. Chen, M. Anpo, J. Phys. Chem. C, **112**, 17809 (2008).
[20] F. Vaja (Dumitru), D. Ficai, A. Ficai, O. Oprea, C. Guran, J. Optoelectron. Adv. Mater,
    15(1- 2), 109 (2013).
[21] H. Zhang, S.C. Wang, D. Xue, Q. Chen, Z.C. Li, Journal of Physics: Conference Series
    152, 012070 (2009)
[22] W. Feng, L. D. Sun, Y. W. Zhang and C. H. Yan, Coord. Chem. Rev., **254**, 1038 (2010)

[23] Hamid Reza Pouretedal, Sara Basati, Iranian Journal of Catalysis **2**(2), 51 (2012).

[24] J. Strunk, W.C. Vining, A.T. Bell, J. Phys. Chem. C **115**, 4114 (2011).

[25] S. Tsunekawa, T. Fukuda, A. Kasuya, J. Appl. Phys. , **87**, 1318 (2000)

[26] S. Gnanam, V. Rajendran, Journal of Sol-Gel Science and Technology, **58**, 62 (2011)

[27] D. Gingasu, O. Oprea, I. Mindru, D. C. Culita, L. Patron, Digest Journal of Nanomaterials and Biostructures – **6**(3), 1215 (2011)

[28] O. Oprea, E. Andronescu, B. S. Vasile, G. Voicu, C. Covaliu, Digest Journal of Nanomaterials and Biostructures, **6**(3), 1393 (2011)

[29] O.R. Vasile, E. Andronescu, C. Ghitulica, B.S. Vasile, O. Oprea, E. Vasile, R. Trusca, Journal of Nanoparticle Research, **14**(12) , art. no. 1269, (2012)

[30] O. Oprea, O.R. Vasile, G. Voicu, L. Craciun, E. Andronescu, Digest Journal of Nanomaterials and Biostructures – **7**(4), 1757 (2012)

[31] G. Voicu, O. Oprea, B.S. Vasile, E. Andronescu, Digest Journal of Nanomaterials and Biostructures, **8**(2), 667 (2013)

[32] O. Oprea, O.R. Vasile, G. Voicu, E. Andronescu, Digest Journal of Nanomaterials and Biostructures, **8**(2), 747 (2013)

[33] H.W. Seo, S.Y. Bae, J. Park, H.N. Yang, K.S. Park, S. Kim, Journal of Chemical Physics, **116**(21), 9492 (2002)